# Rapid and precise scanning helium ion microscope milling of solid-state nanopores for biomolecule detection

**Jijin Yang**[1,4]**, David C Ferranti**[1,4]**, Lewis A Stern**[1]**,
Colin A Sanford**[1]**, Jason Huang**[1]**, Zheng Ren**[2]**, Lu-Chang Qin**[2] **and
Adam R Hall**[3,5]

[1] Carl Zeiss NTS, LLC, One Corporation Way, Peabody, MA 01960, USA
[2] Department of Physics and Astronomy, Curriculum in Applied Sciences and Engineering,
University of North Carolina at Chapel Hill, Chapel Hill, NC 27599, USA
[3] Joint School of Nanoscience and Nanoengineering, University of North Carolina
Greensboro, 2901 E Lee St. Ste 2200, Greensboro, NC 27401, USA

E-mail: adam.hall@uncg.edu

## Abstract
We report the formation of solid-state nanopores using a scanning helium ion microscope. The fabrication process offers the advantage of high sample throughput along with fine control over nanopore dimensions, producing single pores with diameters below 4 nm. Electronic noise associated with ion transport through the resultant pores is found to be comparable with levels measured on devices made with the established technique of transmission electron microscope milling. We demonstrate the utility of our nanopores for biomolecular analysis by measuring the passage of double-strand DNA.

(Some figures in this article are in colour only in the electronic version)

## 1. Introduction

Solid-state (SS) nanopores [1] are among a class of devices capable of biological analysis at the single-molecule level. In this method, an individual, nanometer-scale opening is formed in an otherwise impermeable solid-state membrane that is then placed between two electrically isolated basins of an ionic solution. The application of a voltage difference between the two sides of this membrane sets up an electric field that is highly localized to the interior of the nanopore and is capable of transporting charged molecules through it electrophoretically. The temporary presence of a passing molecule inside the nanopore has been shown to perturb the transmembrane ionic current in a highly repeatable manner, offering a potential means by which to interrogate that molecule. This technique has been used successfully to detect properties of various biomolecules including DNA [2, 3], RNA [4], proteins [5, 6]

and nucleoprotein filaments [7, 8] and holds great potential [9] for future genetic and epigenetic analysis schemes.

To this point, a limited number of reliable single-nanopore formation methods have been reported. The two most widely used techniques are sculpting with a low energy ion beam and sputtering with a transmission electron microscope (TEM). In the former method, an ion sputtering system is used to controllably close a preformed opening of initial diameter ∼100 nm in a silicon nitride substrate [10]. Using a feedback system capable of accurately detecting transmitted ion flux [11], single nanopores were produced with diameters as low as 1–2 nm. In the latter method, the tightly focused beam of a TEM is used to locally ablate a thin, free-standing solid-state membrane [12], resulting in an individual nanopore. Subsequent exposure with a beam of reduced energy can then be used to fluidize the membrane, slowly closing the pore to nearly any size with single nanometer precision [13]. The high degree of controllability afforded by these two methods has allowed for a wide range of studies, including measurements through openings with sizes at or below the cross-sectional
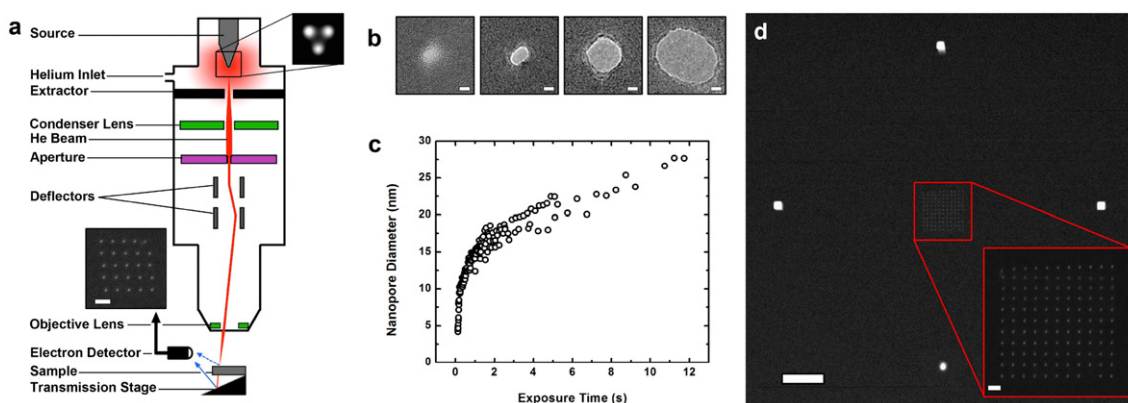
**Figure 1.** HIM nanopore formation. (a) Schematic diagram of the scanning helium ion microscope, showing the beam path from the source to the sample. Top inset shows an image of the three atoms of the source material ('trimer') forming the source tip. Conventional imaging (blue dashed arrow) of secondary electrons is used to optimize beam conditions on the sample. Detection of secondary electrons from an underlying transmission stage (solid blue arrow) can be used to image resultant nanopores *in situ*. Bottom inset shows an example transmission image of a fabricated 5 × 5 array of ∼5 nm diameter nanopores (scale bar is 50 nm). (b) Transmission electron micrographs of four example nanopores formed with HIM milling, with average diameters of (L–R) 3.7, 6.8, 14.6 and 25.8 nm, respectively. Scale bars represent 5 nm. (c) Helium ion beam exposure time versus average diameter of the resultant nanopores (as measured from TEM images) for 162 individual pores fabricated with an ion beam current of 5 pA. (d) Transmission mode HIM image of an 11 × 11 array of 5 nm diameter nanopores (write time approximately 1 min) surrounded by four patterns of ∼100 nm dimensions each. Scale bar represents 500 nm. Inset: a magnified view of the central nanopore array (scale bar is 50 nm).

diameter of the molecule being translocated [14–16]. However, this flexibility comes at the expense of throughput. In both techniques, only a single device chip can be processed at a time and the nanopore shrinking process is reported to take from minutes [10] to over an hour [13]. Considering preparation and pumping time, this puts a practical limit on the number of samples that can be fabricated in a given time.

An ideal solution would be a rapid, direct patterning process with the capability of handling many sample chips at once while maintaining high fabrication resolution. Efforts towards this end have been reported, especially using focused-ion-beam (FIB) milling techniques. While sub-5 nm pore formation has been demonstrated in SiC membranes, these devices have not been used successfully for biomolecular analysis [17, 18], calling into question their efficacy. FIB nanopores made in SiN membranes have shown more utility towards this end, but are generally capable of reaching diameters only as low as 10–20 nm with a single, direct exposure [18, 19]. Gas-assisted FIB was used to fabricate pores as small as 5 nm in diameter [20], but convincing effort was not made to ensure that these were through holes, and thus their use in conventional experiments is unknown. Another method reported nanopores as small as 5.5 nm but resulted in Pt deposits at the nanopore walls [21], which may have important electrochemical implications in future experiments. Here, we present a fast, one-step process for fabricating nanopores in a solid-state membrane using a commercial scanning helium ion microscope [22] (HIM, figure 1(a)), the Carl Zeiss Orion Plus operating with an accelerating voltage of typically 30–35 kV. This instrument uses a source with an atomically small tip (figure 1(a), top inset) to form a helium ion beam with high current and a probe size of ∼0.5 nm. With it, we are able to fabricate nanopores below 4 nm in diameter in unprocessed SiN membranes. Because our method utilizes particle-beam-based lithographic patterning, it is amenable to array formation

and a large sample chamber with stage motion allows multiple samples to be handled without loading/unloading cycles.

## 2. Nanopore formation

For our technique, free-standing SiN membranes supported across a window in a silicon chip are purchased commercially (Protochips, Raleigh, NC). Each chip is rinsed with acetone and ethanol and dried under nitrogen flow before being mounted on a custom HIM sample holder. Our present holder can handle eight individual chips, but we are limited only by the 50 mm travel of the $X$–$Y$ sample stage. With the current size of our silicon support chips, this should allow up to 100 individual SiN membrane chips to be loaded at once. The holder containing the samples is treated with oxygen plasma (150 W) for 5 min and immediately loaded into the HIM sample exchange chamber, where it is exposed to an additional (integrated) air plasma (10 W) for 3 min to ensure minimal contamination before being loaded into the main chamber.

Upon loading the samples, beam conditions are set by adjusting the condenser lens, helium gas flow and aperture (figure 1(a)). For the experiments presented here, the HIM beam current is adjusted to 5 pA through a 10 $\mu$m aperture. Directly prior to pore formation at each sample window, beam focus and stigmation are optimized at a nearby area of the substrate. A brief (∼10 s) single spot exposure of the beam results in a milled mark on the surface that can be used as a feature to tune these conditions using conventional imaging mode (figure 1(a), dashed blue arrow). Once corrected, the beam is blanked and the SiN membrane is moved into the beam path. Here, a computer-controlled exposure of a set time is performed, ablating material and forming the nanopore(s). After exposure, if desired, the resultant milled pattern can then be imaged directly using a transmission stage. With

transmission imaging, secondary electrons are recorded from a metal surface below the thin SiN membrane (figure 1(a), solid blue arrow) rather than from the membrane itself. The presence of an opening in the membrane results in a larger number of transmitted ions and thus greater secondary electron emission, creating a bright spot in the image (figure 1(a), bottom inset). We find insufficient contrast to perform conventional imaging of nanopores, as the membrane itself does not result in enough secondary electrons. For the experiments presented here, we avoid post-fabrication HIM imaging, as the ion beam may have effects on the resultant nanopore size and shape [19]. Instead, we analyze our nanopores using a TEM (JEOL 2010F-FasTEM) set at an accelerating voltage of 120 kV, which is generally unable to modify the SiN.

We find that the exposure time (i.e. exposure dose at constant beam current) of the HIM beam can be used to control nanopore diameter. Figure 1(b) shows four example TEM images of nanopores fabricated with increasing amounts of exposure time. In each case, the opening is clear in the image, with the smallest nanopore observed[6] having a diameter of 3.7 nm (figure 1(b), left), though we note that nanopores of even smaller diameters may be attainable through further variation of microscope conditions (e.g. beam current, aperture, etc). For each nanopore, we measure the area of the opening and calculate an average diameter assuming a perfectly circular pore. We find that the average diameter of HIM-milled nanopores rises quickly and gradually slows with increasing exposure time (figure 1(c)). We also find a narrow distribution of diameters ($\pm 3$ nm on average) resulting from a given exposure. This indicates a high level of control over nanopore dimensions is attainable simply by adjusting the exposure time appropriately, suggesting that HIM milling can be used as a highly repeatable fabrication process. Furthermore, due to the lithographic nature of the process used here, we also note that large-area arrays can be made quickly while retaining the range of attainable nanopore diameters (figure 1(d)).

It has been shown [23] that ion milling can be described generally by the equation

$$\log(d) = a + b\log(D)$$

where $d$ is the feature dimension (in this case, nanopore diameter), $D$ is ion dose and $a$ and $b$ are correlation constants. We therefore expect a linear relation between total ion dose and resultant nanopore diameter on a log–log scale. However, such a plot (figure 2(a)) actually shows two distinct linear regimes: a fast rate below a diameter of $\sim 10$ nm (I) and a slower rate above that diameter (II). We account for this observation by considering nanopore shape. For nanopores with small diameter relative to the beam size, it has been observed [24] that membrane thickness decreases gradually, leading inward towards short interior sidewalls (figure 2(b), I) due to the fast (Gaussian) decrease of intensity measured radially from the center of the impinging beam. During milling at this stage,

---

[6] We note that shorter exposure times resulted in nanopores of smaller apparent size, but we were unable to confirm that they were indeed through holes, and so we do not consider these here.
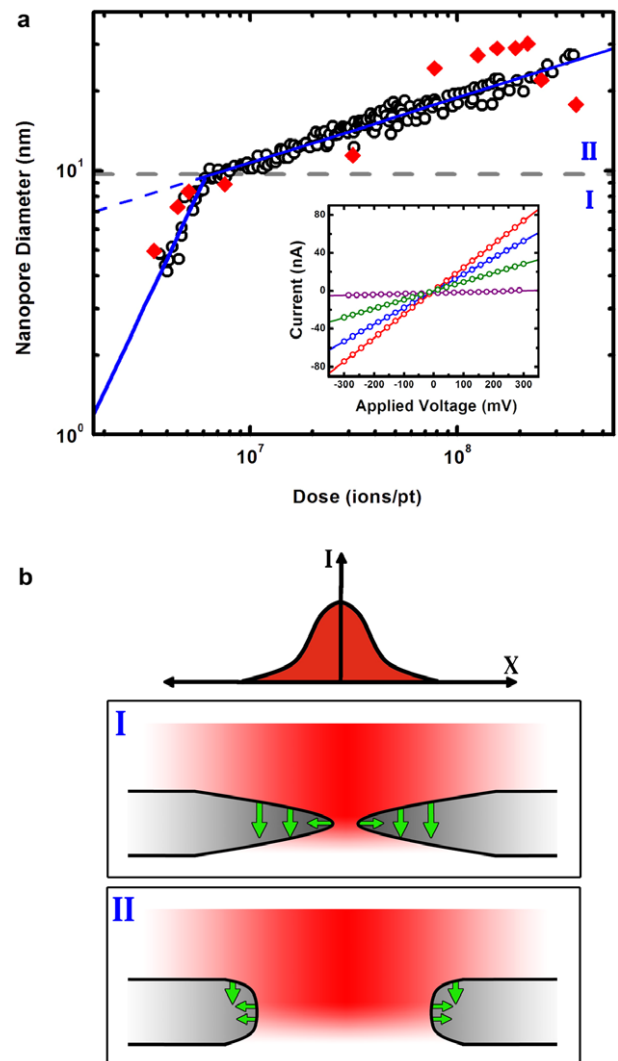


**Figure 2.** Formation regimes and ionic current measurement. (a) Log–log plot of helium ion dose versus resultant nanopore diameter showing two distinct rate regimes; one below $\sim 10$ nm (I) and one above (II). Blue lines are a linear fit to the data on the log scale. Red diamonds represent nanopore diameters calculated from ionic current measurements through individual nanopores. Inset shows linear $I$–$V$ curves obtained from four typical nanopores with calculated diameters of 29 (red), 25 (blue), 18 (green) and 5 nm (purple), respectively. (b) Diagrammatic representation of the high (I) and low (II) milling rate regimes (top: Gaussian intensity profile of the ion beam). In regime I, the sloped membrane around the nanopore leads to a mostly direct beam incidence and therefore a high pore growth rate. In regime II, the flat sidewalls of the nanopore lead to a grazing incidence of the beam, reducing the total milling yield and thus the pore diameter growth rate.

there is a relatively high yield over most of the membrane surrounding the nanopore opening. However, as the nanopore diameter increases, the reduction in surrounding membrane thickness becomes more severe, resulting in longer interior sidewalls [24] (figure 2(b), II). In this case, the milling yield at the interior walls of the nanopore is low, since the ion beam strikes them at a grazing angle [25, 26]. This, combined with the loss of yield caused by the central part of the beam passing through the nanopore opening, results in a significantly lower

overall growth rate of the pore. We therefore interpret the transition from regime I to regime II as a transition in nanopore shape from a short interior sidewall to a longer one.

## 3. Noise analysis and DNA translocations

We now evaluate the utility of our devices for conventional nanopore experiments. In order to do this, single nanopores of varying size are fabricated in separate device chips. Each chip is treated on both sides with an oxygen plasma (100 W) before being immediately loaded into a Perspex flow cell containing two chambers with access to either side of the membrane. We then introduce an electrolyte solution containing 1 M KCl, 10 mM tris-HCl (pH 8.0) and 1 mM EDTA to each compartment and make electrical contact using Ag/AgCl electrodes attached to a patch clamp amplifier (Axon 200B, Axon Instruments) for current measurement. HIM-milled nanopores exhibit linear $I$–$V$ curves (figure 2(a), inset), like those measured in other methods [18, 27]. We find that the measured conductance $G$ of a given nanopore varies with the total ion dose used to form it. This conductance can be used to calculate the apparent diameter $d$ of each nanopore using a simplified model [27]:

$$G = \frac{\pi}{4} \frac{d^2}{L} \left( (\mu_K + \mu_{Cl}) n_K e + \mu_K \frac{4\sigma}{d} \right)$$

where $L$ is the length of the nanopore, $\mu_K$ and $\mu_{Cl}$ are the electrophoretic mobilities of potassium and chloride (7.616 and $7.909 \times 10^{-8}$ m$^2$ V$^{-1}$ s$^{-1}$, respectively), $n_K$ is the number density of counterions, $e$ is the elementary charge and $\sigma$ is the surface charge density of the nanopore material. Here, we take $L$ to be the thickness of the membrane (42.7 nm, as measured by ellipsometry) and $\sigma$ as 60 mC m$^{-2}$, following [27]. Using this, we can now plot the calculated nanopore diameter as determined from the measured ionic transport against the ion dose used in formation. Doing so (figure 2(a)), we find good agreement with the trend identified through TEM imaging. We attribute the somewhat larger variation of these calculated values to our inability to take into account factors like variation in pore shape (roundness, etc).

An important aspect of these ionic transport measurements is the noise associated with them. The noise levels in TEM nanopores, for example, has been widely studied [14, 28–30] because signal-to-noise ratio is of central concern to their use in biomolecule detection [31]. We therefore analyze the current noise in our HIM nanopores and compare them directly with ones formed by TEM in the same type of membrane. For these measurements, 100 mV was applied and current was measured across the pore at a rate of 200 kHz and low pass filtered at 100 kHz before being digitized. Figure 3(a) shows the current power spectral density (PSD) for both a TEM and an HIM pore, each with a diameter of about 12 nm. The cross-spectral noise properties between the two are similar, with the TEM nanopore level being slightly lower than that of the HIM nanopore in the intermediate frequency range. By calculating the mathematical integral of the PSD for multiple individual samples made with both methods (figure 3(b)), we find that current noise in fact follows the same general trend in both
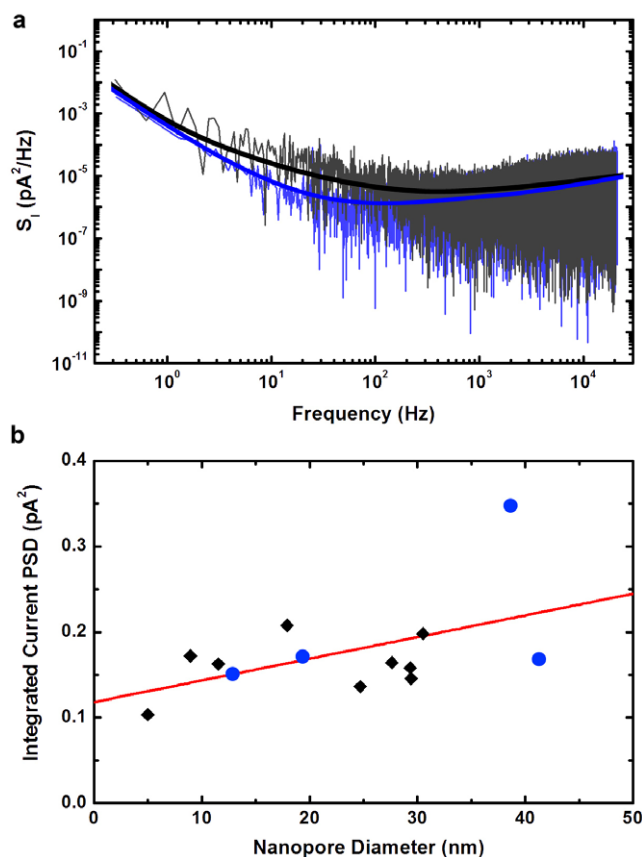


**Figure 3.** Ionic current noise analysis. (a) Comparison of current power spectral density (PSD) for a HIM-milled nanopore (black) and a TEM-milled nanopore (blue), showing comparable cross-spectral noise levels at 100 mV applied voltage. Both pores were ~12 nm in diameter and the solid line is a spline fit to the data in order to make both trends clear. (b) Comparison of the integrated current PSD at 100 mV applied voltage for HIM nanopores (black diamonds) and TEM nanopores (blue circles) with various diameters, showing the same trend. The red line is a linear fit to all points and is intended as a guide to the eye.

cases. From this, we can say that the ionic current noise for HIM nanopores is comparable to that of TEM nanopores.

Finally, we show that nanopores formed with the HIM milling method are capable of biomolecule detection by measuring double-strand (ds) DNA translocations. This is the molecule most widely studied with solid-state nanopores, and can thus be considered a standard. For the experiment, we use a nanopore with diameter 24.7 nm, cleaned prior to measurement in the same way as described above. Initial characterization shows linear $I$–$V$ characteristics with a resistance of 5.6 M$\Omega$ and current noise comparable to that discussed above. Next, $\lambda$ dsDNA (48.5 kb) is loaded into the *cis*-chamber (figure 4(a)) at a concentration of ~300 ng $\mu$l$^{-1}$. The subsequent application of a transmembrane voltage results in a series of downward spikes in the measured nanopore conductance (figure 4(b)), characteristic of dsDNA translocations. Closer analysis (figure 4(c), left) reveals structure within these events that is caused by different folding conformations of the molecule during translocation [2, 3]. Indeed, a histogram of all conductance data points (figure 4(c), right) shows that
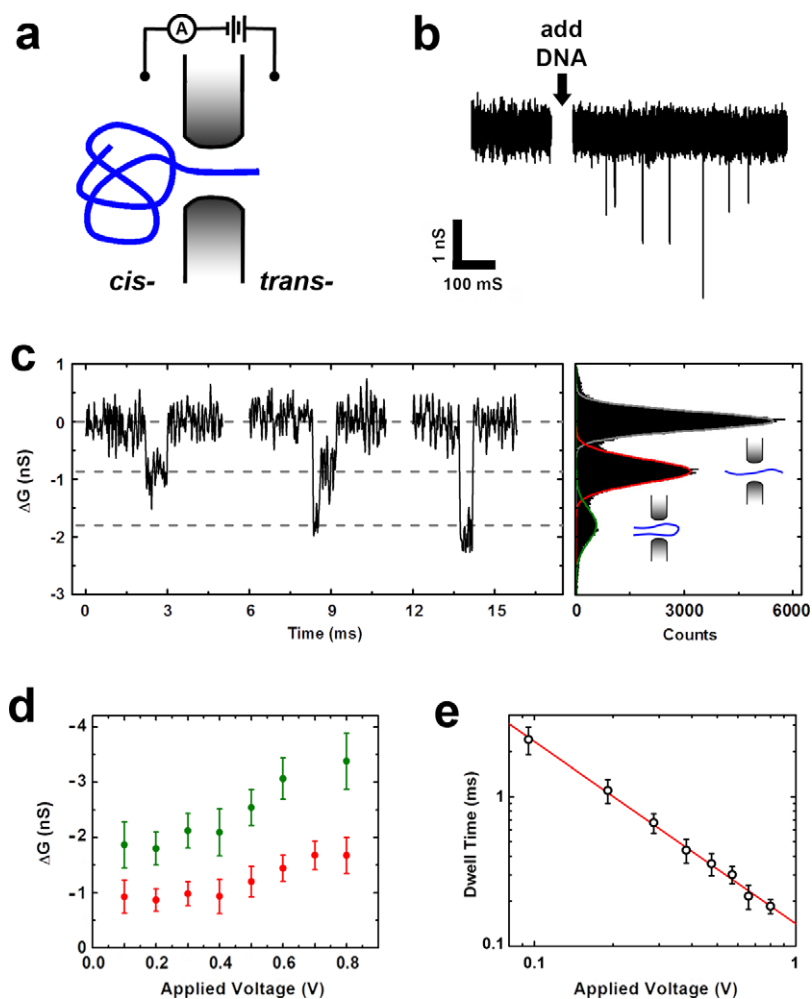
**Figure 4.** DNA transport through HIM nanopores. (a) Schematic representation of the DNA translocation measurement. (b) A typical measured conductance trace ($V_{app} = 200$ mV, low pass filtered at 10 kHz) revealing downward spikes after the addition of dsDNA. (c) The panel at left shows examples of individual events ($V_{app} = 200$ mV, low pass filtered at 10 kHz), indicating the translocation of unfolded (left), partially folded (center) and folded dsDNA (right). The panel at right shows a histogram of all measured conductance points for 878 individual events. Insets show diagrammatic explanation of the adjacent peaks. (d) Average conductance blockade level (mean of the Gaussian fit to the histogram) for unfolded (red) and folded (green) dsDNA over a range of applied voltage. The histograms from 100 to 800 mV were composed of individual events numbering 508, 878, 1101, 914, 1331, 1398, 1467 and 1440, respectively. Error bars denote the sigma of the Gaussian fits. (e) Log–log plot of average event dwell time versus applied voltage. Only unfolded translocations were considered. The red line is a linear fit to the data.

the measured conductance levels fall into easily separable populations. The HIM nanopore was sufficiently stable to perform this measurement over a large range of applied voltage (100–800 mV), resulting in a total of over 9000 individual recorded events. Figure 4(d) shows the depth ($\Delta G$) of both the unfolded and singly folded conductance levels. We observe an increase in the depths of both types of events over the voltage range, in qualitative agreement with the trend found previously for unfolded translocations [4]. We also note that the measured dwell time of events (i.e. the time from the initial conductance drop to its return to the baseline value) exhibits a clear $1/V$ dependence (figure 4(e)), as has been observed previously [7].

## 4. Conclusions

In conclusion, we have demonstrated the controlled fabrication of solid-state nanopores in thin SiN membranes using a

scanning helium ion microscope. The method is highly repeatable and can achieve diameters as low as 4 nm reliably, or about 60% smaller than other one-step ion milling techniques. We showed that nanopores formed with this method are capable of ionic transport and that the current noise properties are comparable to those of pores fabricated with a TEM. Finally, we demonstrated the efficacy of HIM nanopores in biomolecule detection experiments by performing dsDNA translocations. We observed indications of DNA folding and a high level of stability, recording of over 9000 individual events over a large range of applied voltage. Our method is fast— seconds of exposure even for a pore with fairly high diameter— and even with the large range of attainable diameters, can produce nanopore arrays of considerable size in a brief time. The technique also allows multiple samples to be loaded into the fabrication chamber at once, reducing preparation and exchange time. Considering these factors, our HIM method

improves the throughput of samples significantly and may allow for the production of small nanopores at the wafer scale.

## Acknowledgments

## References

[1] Dekker C 2007 *Nat. Nanotechnol.* **2** 209
[2] Li J L, Gershow M, Stein D, Brandin E and Golovchenko J A 2003 *Nat. Mater.* **2** 611
[3] Storm A J, Chen J H, Zandbergen H W and Dekker C 2005 *Phys. Rev.* E **71** 051903
[4] Skinner G M, van den Hout M, Broekmans O, Dekker C and Dekker N H 2009 *Nano Lett.* **9** 2953
[5] Firnkes M, Pedone D, Knezevic J, Doblinger M and Rant U 2010 *Nano Lett.* **10** 2162
[6] Talaga D S and Li J L 2009 *J. Am. Chem. Soc.* **131** 9287
[7] Kowalczyk S W, Hall A R and Dekker C 2010 *Nano Lett.* **10** 324
[8] Smeets R M M, Kowalczyk S W, Hall A R, Dekker N H and Dekker C 2009 *Nano Lett.* **9** 3089
[9] Branton D *et al* 2008 *Nat. Biotechnol.* **26** 1146
[10] Li J, Stein D, McMullan C, Branton D, Aziz M J and Golovchenko J A 2001 *Nature* **412** 166
[11] Stein D M, McMullan C J, Li J L and Golovchenko J A 2004 *Rev. Sci. Instrum.* **75** 900
[12] Storm A J, Chen J H, Ling X S, Zandbergen H W and Dekker C 2005 *J. Appl. Phys.* **98** 014307
[13] Storm A J, Chen J H, Ling X S, Zandbergen H W and Dekker C 2003 *Nat. Mater.* **2** 537
[14] Mirsaidov U, Comer J, Dimitrov V, Aksimentiev A and Timp G 2010 *Nanotechnology* **21** 395501
[15] van den Hout M, Krudde V, Janssen X J A and Dekker N H 2010 *Biophys. J.* **99** 3840
[16] Wanunu M, Sutin J, McNally B, Chow A and Meller A 2008 *Biophys. J.* **95** 4716
[17] Gierak J *et al* 2007 *Microelectron. Eng.* **84** 779
[18] Schiedt B *et al* 2010 *Microelectron. Eng.* **87** 1300
[19] Lo C J, Aref T and Bezryadin A 2006 *Nanotechnology* **17** 3264
[20] Spinney P S, Howitt D G, Smith R L and Collins S D 2010 *Nanotechnology* **21** 375301
[21] Chen P, Wu M Y, Salemink H W M and Alkemade P F A 2009 *Nanotechnology* **20** 015302
[22] Morgan J, Notte J, Hill R and Ward B 2006 *Microsc. Today* **14** 8
[23] Tseng A A 2005 *Small* **1** 924
[24] van den Hout M, Hall A R, Wu M Y, Zandbergen H W, Dekker C and Dekker N H 2010 *Nanotechnology* **21** 115304
[25] Tseng A A 2004 *J. Micromech. Microeng.* **14** R15
[26] Wetz P, Kruger W, Scharmann A and Schartner K H 1997 *Radiat. Meas.* **27** 569
[27] Smeets R M M, Keyser U F, Krapf D, Wu M Y, Dekker N H and Dekker C 2006 *Nano Lett.* **6** 89
[28] Hoogerheide D P, Garaj S and Golovchenko J A 2009 *Phys. Rev. Lett.* **102** 256804
[29] Smeets R M M, Dekker N H and Dekker C 2009 *Nanotechnology* **20** 095501
[30] Smeets R M M, Keyser U F, Dekker N H and Dekker C 2008 *Proc. Natl Acad. Sci. USA* **105** 417
[31] Tabard-Cossa V, Trivedi D, Wiggin M, Jetha N N and Marziali A 2007 *Nanotechnology* **18** 305505